Science Advances
AAAS

advances.sciencemag.org/cgi/content/full/6/5/eaaz3194/DC1

Supplementary Materials for

Low-power microelectronics embedded in live jellyfish enhance propulsion

Nicole W. Xu and John O. Dabiri*

*Corresponding author. Email: jodabiri@caltech.edu

Published 29 January 2020, *Sci. Adv.* **6**, eaaz3194 (2020)
DOI: 10.1126/sciadv.aaz3194

The PDF file includes:

Other Supplementary Material for this manuscript includes the following:

(available at advances.sciencemag.org/cgi/content/full/6/5/eaaz3194/DC1)

Movie S1 (.mov format). A comparison of bell geometries for unstimulated swimming with an inactive swim controller embedded (left) and externally controlled swimming at 0.50 Hz (middle) and 0.88 Hz (right).

Supplementary Text

Extended results: Characterizing animal response to electrical signals

For a range of square pulse widths from 1.0 to 10.0 ms (Table S1), tested at 1.00 Hz and 4.2 V, the peak frequency of the mean SSAS was consistently at 1.00 ± 0.06 Hz (within the 0.06-Hz windowing error) for N = 6, 5, 10, and 5 animals, respectively. At the two extremes, 0.1 and 90.0 ms, the peak frequency was 0.71 ± 0.18 Hz for N = 6 and 4. Tissue damage also occurred at waveform durations greater than 10.0 ms, so it is hypothesized that localized muscle injury can inhibit effective signal transmission. For the range of signal amplitudes between 0.1 and 4.2 V (Table S1), tested at 1.00 Hz with a 4.0 ms pulse width, the peak frequency occurred at 1.00 ± 0.06 Hz (for sequential N = 10, 5, 9, 4, 10, and 10 animals), with no observed tissue damage. This suggests a wide range of voltages to stimulate muscle contractions, with a lower bound on the signal pulse width to activate contractions, and an upper bound on the width to prevent muscle damage.

Therefore, we conclude that external muscle stimulation is robust for a wide range of electrical signals tested, with minimal to no tissue damage. Effective stimulation parameters for controlled *A. aurita* muscle excitation include a voltage range of 0.1-4.2 V and pulse widths of 1-10 ms. Damage was observed to occur at longer pulse widths.

However, animals failed to respond to stimulation frequencies higher than 1.50 Hz, due to limits imposed by the refractory period of the muscle. Interestingly, consistent muscle contractions were observed above the theoretical limit reported by Bullock (*32*), which suggests that the absolute refractory period is shorter than estimated from endogenous contractions.

Extended results: Immunohistochemical staining and implications on electrode placement

Electrode placement was tested at four locations along the subumbrella (at a given signal of 4.2 V, 4.0 ms, and 1.00 Hz), as shown in Fig. 2A. The peak frequency for all mean SSAS curves was 1.02 Hz, within the windowing error of 0.02 Hz.

Actin stains of the swim muscle showed that the muscle monolayer extends fully toward the gastric pouch regions. Therefore, electrodes at all locations were in contact with the muscle. There was no clear distinction between radial and circumferential muscles, although there was a gradual transition from wavelike striation patterns (Fig. S1A) toward the center of the bell, to more purely circumferential striations midway between the gastric pouches and the bell margin (Fig. S1B), and entirely circumferential orientations at the margin (Fig. S1C). The wavelike pattern near the gastric pouches likely reflects tissue deformation due to residual stress following excision.

Muscle stains at the subumbrellar surface suggest a gradual transition between radial and circumferential muscles, if any differentiation of the two muscle groups can be classified at all. Previously, the entire spatial organization of subumbrellar muscles has been characterized in ephyrae (juvenile jellyfish) and smaller medusae (up to 4.0 cm), with a clear distinction between coronal and radial muscle (*39*). It is known that the radial muscles and circumferential muscles in ephyrae exist in distinct bands and junctions, and that these bands do not fill the entire subumbrellar surface (*9*). Hence, the present results indicate an ontogenetic transition in muscle morphology. A limitation of the present staining protocol is that tissue excision removes the

pressure from surrounding tissue in intact medusae, leading to observed tissue deformation from residual stress.

Those limitations notwithstanding, the presence of striated muscle at all locations from the gastric pouches to the rhopalia confirms that electrical stimulation is directly transmitted to the muscle, in addition to transmission via nerve nets. This simplifies attaching the swim controller because the effect on muscle contractions is spatially nonspecific on the subumbrellar surface, so free-swimming experiments were done by inserting electrodes toward the bell margin, but not at the margin where tissue depth is too minimal to ensure that the electrode is properly secured.

Extended results: Model parameters sweeps

To quantitatively characterize these observations and their dependencies on individual parameters of body morphology and stimulation, we modeled jellyfish motion using a momentum balance incorporating thrust, drag, acceleration reaction, and inertial forces (for additional details, see "Mechanistic model" in Materials and Methods) (*20, 42*).

Note that our model separates swimming into two regimes consistent with empirical observations. Specifically, when the stimulation frequency is below the biological maximum, i.e., $f \leq f_{crit}$, the bell contracts and then coasts until the subsequent contraction. When the stimulation frequency is too high, i.e, $f > f_{crit}$, bell relaxation is interrupted by the next contraction (Fig. S2; see also Movie S1).

To deduce how individual morphological and kinematic parameters affected the relative swimming speeds, we conducted parameter sweeps for frequencies from 0.25 to 1.00 Hz (Table S2). Four representative parameter sweeps are illustrated in Fig. S3 (additional sweeps in Fig. S4). Overall, performance enhancement was amplified for cases with maximal changes in subumbrellar cavity volume between relaxation and contraction, for a given fineness ratio (Fig. S3A). However, morphological and kinematic parameters could affect swimming speeds proportionally (Fig. S3C), nonlinearly (Fig. S3D), or shift the frequency at which peak enhancement occurred (Fig. S3B). The combined effects of changes in multiple parameters could therefore result in non-monotonic trends. Both empirical data and theoretical analysis suggest that smaller animals with less oblate bell morphologies have the greatest capacity for latent enhanced propulsion. Interestingly, this observation is consistent with the known behaviors of small, prolate hydromedusae such as *Leuckartiara* sp., which use short bursts of high swimming speed to catch prey and escape predation (*38*).

Limitations

Endogenous animal contractions can result in multiple contractions per input signal (Fig. 2C, $t \approx$ 12 s). Similarly, all baseline measurements at 0 Hz (no stimulation) still resulted in native animal contractions and forward motion. Because there has been no reported method of arresting endogenous signals immediately (we tested muscle relaxants such as menthol and $MgCl_2$; however, both were slow to take effect and wear off) or entirely without tissue excision, muscle responses are a combination of both endogenous and external stimuli. This is especially apparent for 0.25-Hz external stimulation, which suggests a lower limit for external frequency stimulation with the present approach, although lower frequencies can still be used if the presence of endogenous signals is acceptable. Furthermore, basal metabolism without muscle contractions could not be measured because the presence of menthol and $MgCl_2$ to arrest motion also affected

the fidelity of oxygen measurements. Further partitioning of the animal energy consumption between swimming and other life functions remains a focus on future work.
An additional limitation exists for all oxygen consumption measurements. Because forward motion is restricted to enable metabolic measurements in an enclosed metabolic chamber (Fig. 5), altered swimming kinematics could affect oxygen consumption. However because the experimental values matched the predicted values from three separate methods, including theoretical predictions for energy consumption by freely swimming animals, these effects appear negligible.

Ethical considerations

A. aurita are invertebrate animals with no central nervous system or reported nociceptors. However, we took steps to ensure that no unnecessary tissue damage occurred during experiments. Initial swim controller designs used Histoacryl® Flexible (B. Braun Medical Inc., Bethlehem, PA, USA) and mussel-inspired adhesives (*43*) as superficial attachment methods instead of an embedded wooden pin. However, these methods were difficult to use because they required the tissue to be dry upon initial attachment, and could not sustain tissue contact after minutes of animal swimming. Thus, the swim controller we present uses a thin wooden pin that embeds into the bell. Animals were allowed to rest between subsequent experiments, and physical damage from the embedded portion healed within days. Two animals for the free-swimming experiments exhibited abnormal muscle wave propagations in response to a high stimulation frequency (>0.75 Hz), in which the muscle contraction propagated unidirectionally and continuously, but returned to exhibit normal contraction patterns within hours to two days, at maximum. All animals recovered post-experiments, although some with bell deformities due to being constrained in a rectangular tank with still water, instead of a constant flow pseudokreisel tank, for over 24-36 hours.

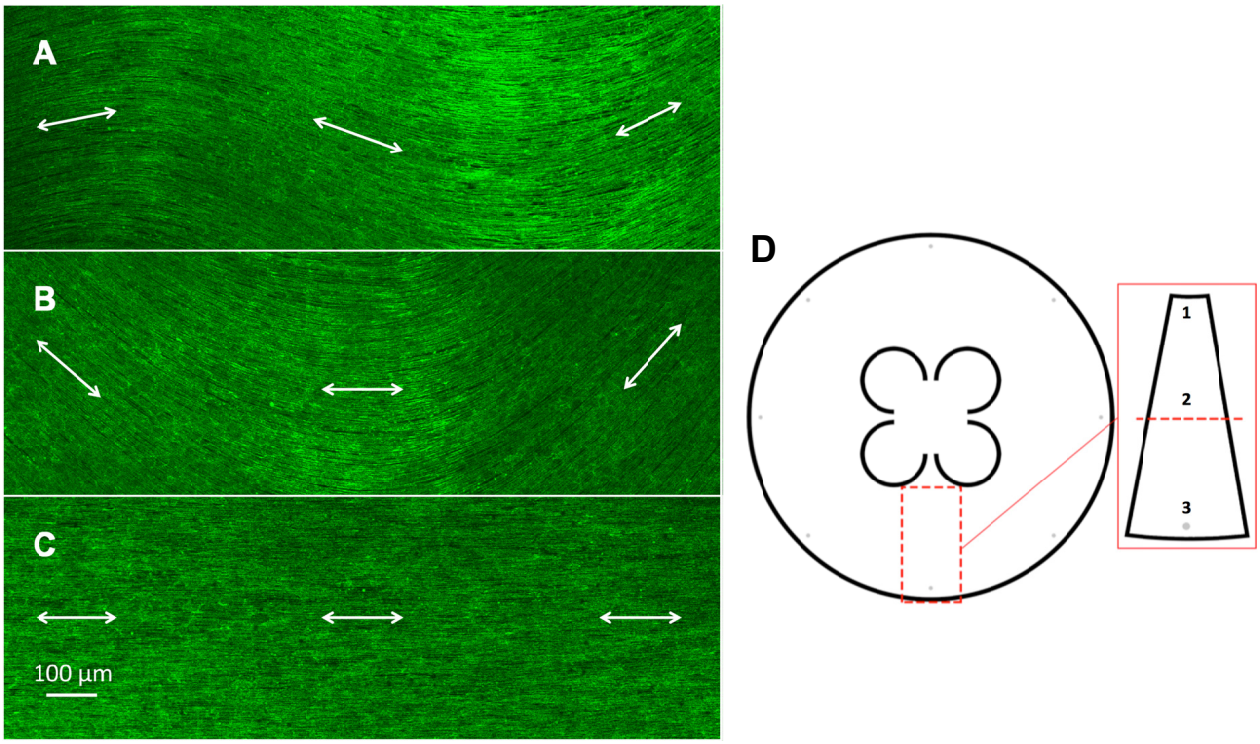

Fig. S1. Muscle orientation along the subumbrellar surface. Actin-phalloidin stain along the centerline of jellyfish tissue from the gastric pouch to the margin to visualize the spatial orientation of muscle striations in 7.0-10.0 cm diameter *Aurelia aurita* medusae. (**A**) An innermost section of tissue near the gastric pouch, corresponding with point 1 in the inset schematic in (D), showing a wavelike pattern. (**B**) A midsection of tissue, corresponding with point 2, showing the transition from wavelike bands to a more circumferential orientation. (**C**) An outermost section of tissue near the margin, corresponding with point 3, showing a purely circumferential orientation that aligns with the horizontal edge of the tissue (not shown). (**D**) Cartoon illustrating the cut section of tissue for staining.

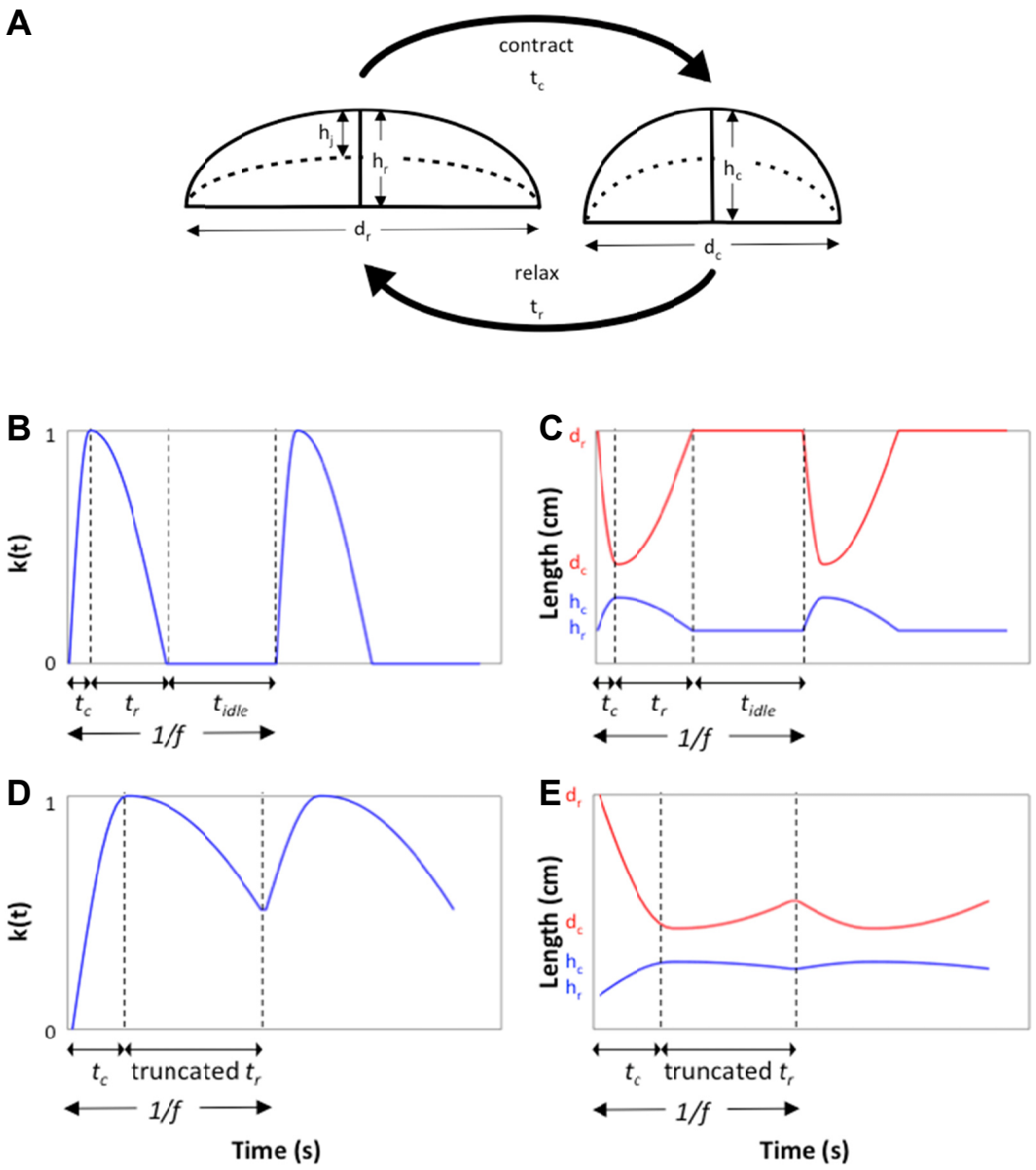

Fig. S2. Details of the adapted hydrodynamic model. (**A**) Sagittal plane view of the model jellyfish bell, idealized as an oblate hollowed hemiellipsoid defined by the following geometric parameters. In its relaxed state (left), the bell is characterized by height (h_r), diameter (d_r), and jellyfish tissue depth at the axial center (h_j). In its contracted state (right), the bell is characterized by height (h_c), diameter (d_c), and the same tissue depth (h_j). The dashed line separates the bell tissue (top) from the subumbrellar volume (bottom). The transition from relaxed to contracted states occurs over the contraction time (t_c), and from contracted to relaxed states over the relaxation time (t_r). The period over one contraction/relaxation cycle is defined as $\tau_{crit} = t_c + t_r$ and $f_{crit} = 1/\tau_{crit}$. To model external swim control, τ_{crit} is independent of the driven frequency (f), which results in two separate swimming regimes over a range of f values: when

$f \le f_{crit}$ in (B) and (C), and when $f > f_{crit}$ in (D) and (E). (**B**) For $f \le f_{crit}$, when the bell is allowed to completely relax within each driven swim cycle, the model uses a Heaviside sinusoid as an input function *k(t)* to calculate changes in bell morphology. For each swim cycle, *k(t)* ramps from 0 to 1 over t_c, decreases over t_r, and remains at 0 for an idle time period ($t_{idle} = 1/f - \tau_{crit}$) before repeating. Two representative periods are shown for simplicity. (**C**) Using this input function *k(t)*, the instantaneous bell diameter and height are calculated as follows: $h_t = h_r + \Delta h\ k(t)$, where the maximum range in height is defined as $\Delta h = h_c - h_r$, and $d_t = d_r - \Delta d\ k(t)$ where the maximum range in diameter is defined as $\Delta d = d_r - d_c$. (**D**) For $f > f_{crit}$ in which the frequency is too high allow for full relaxation, *k(t)* is a truncated Heaviside sinusoid, so a new resting state is defined after the first period. Two representative periods are shown for simplicity, but the *k(t)* for each subsequent contraction is a repeat of the second period. (**E**) Using this input function *k(t)* with a truncated limit, the instantaneous bell diameter and height are calculated using the same equations as in (C).

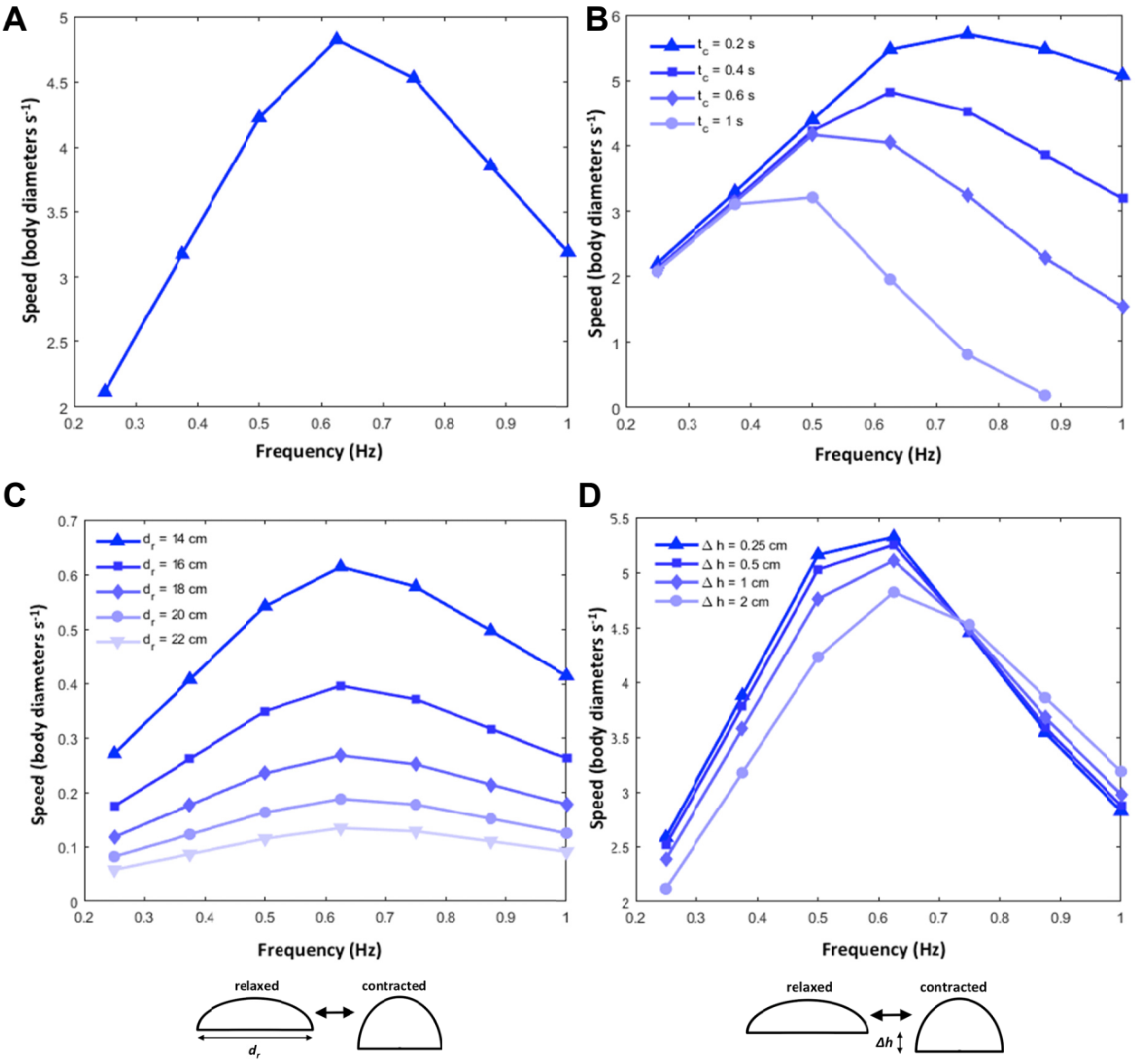

Fig. S3. Parametric dependencies of enhanced propulsion. Normalized swimming speeds (body diameters s^{-1}) for parameter sweeps across a frequency range from 0.25 to 1.00 Hz. See Table S2 for details of the model, and Fig. S4 for additional parameter sweeps. (**A**) Normalized swimming speeds collapse onto a single curve for bell geometries with the same fineness ratio (ratio of height to diameter) but different sizes (i.e., scale factor s = 0.25, 0.50, 1.00, 1.50, and 2.00). A representative curve for s = 1.00 is shown. The peak speed occurs at 0.62 Hz. (**B**) Decreasing the contraction time (t_c) increases swimming speeds, and the frequency at which the peak speed occurs shifts from 0.50 Hz for contraction times of 0.6 and 1.0 s, to 0.62 Hz for 0.4 s, to 0.75 Hz for 0.2 s. In the laboratory, jellyfish have observed contraction times between 0.4 and

1.0 s. (**C**) Increasing the resting body diameter (d_r), which decreases the fineness ratio toward a more oblate shape, decreases overall swimming speeds. The peak speed remains at 0.62 Hz. **(D)** Increasing the change in height between contracted and relaxed states (Δh) decreases the swimming speeds at 0.62 Hz (where the peak speed occurs) and below, and slightly increases the speeds at higher frequencies.

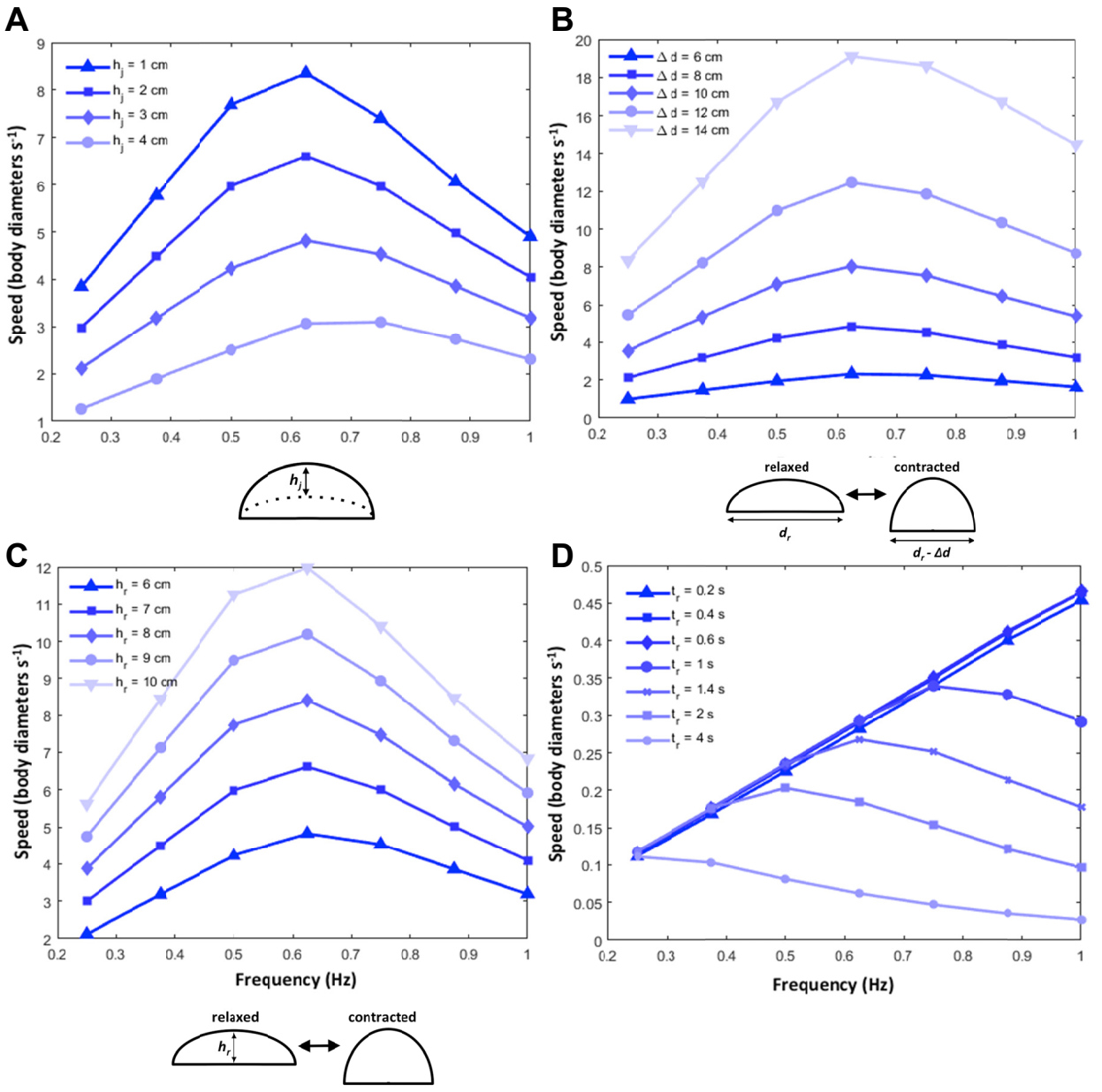

Fig. S4. Additional parametric dependencies of enhanced propulsion model parameter sweeps. (**A**) Normalized speeds (body diameters s^{-1}) for morphological and kinematic parameter sweeps across a frequency range from 0.25 to 1.00 Hz. See Fig. S2 and Table S2 for more details about the model, and Fig. S3 for other parametric sweeps. (A) Increasing the tissue thickness of the jellyfish (h_j) decreases speed and shifts the peak speed toward higher frequencies because of the decrease in subumbrellar cavity volume. (**B**) Increasing the change in body diameter between contracted and relaxed states (Δd) increases speeds, without shifting the peak speed from 0.62 Hz. (**C**) Increasing the resting height of the bell (h_r) to increase the fineness ratio (toward a less oblate bell shape) increases overall speeds. The peak speed remains at 0.62 Hz. (**D**) Increasing the relaxation time (t_r) decreases overall speeds and shifts the curve toward a peak speed at lower frequencies because of time-constrained geometric truncations.

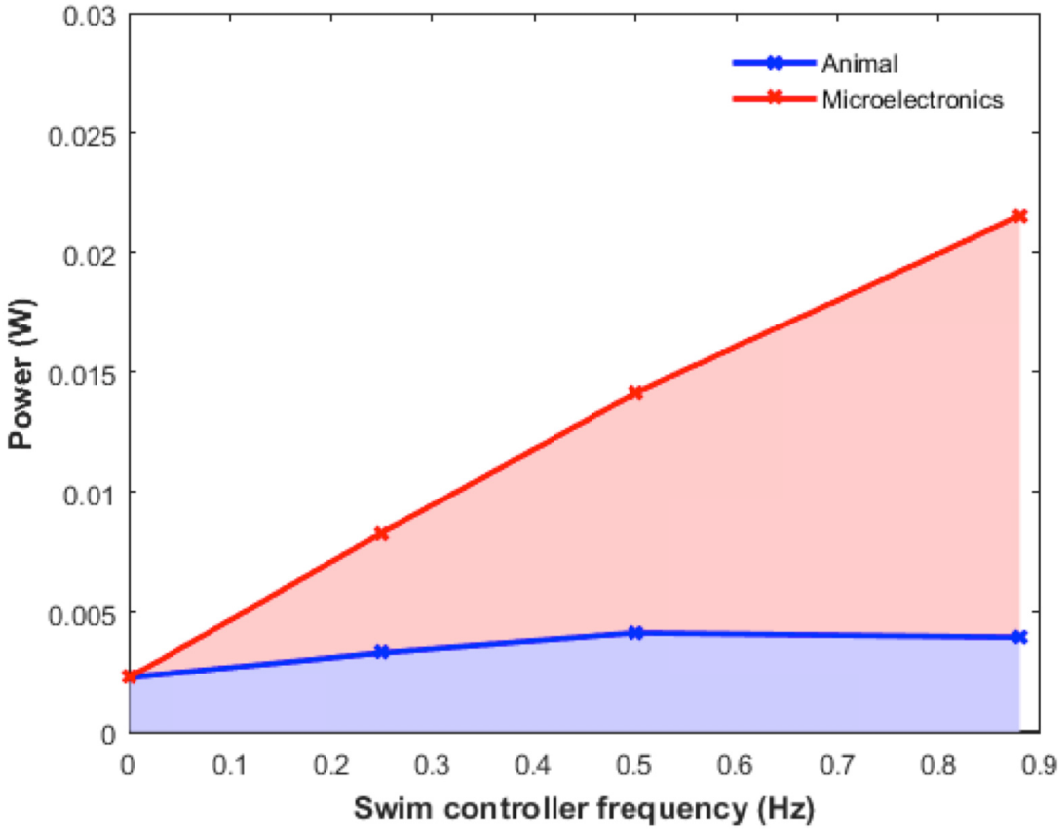

Fig. S5. Power requirements of the microelectronic system versus animal. The blue shaded region illustrates the mean power requirements of the animals (N = 7), using oxygen consumption measurements from respiratory rate experiments at 0 Hz (no stimulation) and 0.25, 0.50, and 0.88 Hz. The red shaded region illustrations the mean power requirements of the microelectronic system as a function of stimulation frequency.

Table S1. Experimental parameters (columns) for each electrical signal characteristic test (rows).

	f: Frequency (Hz)	A: Amplitude (V)	T: Pulse Width (ms)
Signal Frequency Test	0.25, 0.50, 0.75, 1.00, 1.20, 1.50, 2.00, 5.00, 10.00, 90.00	4.2	4.0
Signal Amplitude Test	1.00	0.1, 1, 2.5, 3, 3.7, 4.2	4.0
Signal Pulse Width Test	1.00	4.2	0.4, 1.0, 2.0, 4.0, 10.0, 90.0

Table S2. Model parameters, including the resting body diameter (d_r), range of diameters between relaxation and contraction geometries (Δd), resting body height (h_r), range of height between contraction and relaxation geometries (Δd), tissue height or depth (h_j), contraction time (t_c), relaxation time (t_r), and a geometric scale factor (s) that factors into each geometric parameter proportionally. For all parameter sweeps, average speeds were calculated at frequencies, f = [0.25, 0.38, 0.50, 0.62, 0.75, 0.88, 1.00] Hz.

	Parameters	Fig. Reference
Baseline	Relaxed bell diameter, d_r = 18 cm Change in bell diameter, Δd = 8 cm Relaxed bell height, h_r = 4 cm Change in bell height, Δh = 2 cm Tissue height, h_j = 3 cm Contraction time, t_c = 0.4 s Relaxation time, t_r = 1.4 s Geometric scale factor, s = 1	Fig. S2
Scaling Sweep	s = [0.25, 0.50, 1.00, 1.50, 2.00]	Fig. S3A
Contraction Time Sweep	t_c = [0.2, 0.4, 0.6, 1.0] s	Fig. S3B
Diameter Sweep	d_r = [14, 16, 18, 20, 22] cm	Fig. S3C
Range of Height Sweep	Δh =[0.25, 0.50, 1.00, 2.00] cm	Fig. S3D
Tissue Height Sweep	h_j = [1, 2, 3, 4] cm	Fig. S4A
Range of Diameter Sweep	Δd = [6, 8, 10, 12, 14] cm	Fig. S4B
Height Sweep	h_r = [6, 7, 8, 9, 10] cm	Fig. S4C
Relaxation Time Sweep	t_r = [0.2, 0.4, 0.6, 1, 1.4, 2.0, 4.0] s	Fig. S4D

Table S3. External power per mass calculations of various robotic constructs. Mean values are listed for the biohybrid robot at three externally-driven frequencies (0.25, 0.50, and 0.88 Hz, respectively). External power is calculated as $P = V \times I$, in which V is the measured voltage. and I is calculated by the battery specifications (10 mAh) and lifetime of the device (3.6 hours, from a representative experiment at 0.50 Hz). For a representative calculation of values obtained experimentally, at 0.50 Hz, V is a mean value of 3.7 V and ranges from 2.8-4.2 V, and the lifetime for the device is 3.6 hours, which results in a power of 10 mW. External powers at other frequencies are calculated as $P = V \times I_{\max} \times (duty\ cycle)$, extrapolated using the experimental value at 0.50 Hz to obtain a realistic I_{max}. Note that for all robots with live components (such as cells, tissues, and animals), energy consumption of live tissue is neglected. If external power values were not explicitly stated in literature, power is calculated as $P = V \times I \times (duty\ cycle)$, such as for the medusoid, SoFi, and REMUS 100. Because no mass measurements were provided for the medusoid, mass was estimated to be 1 g to give a conservative external power per mass. Two values are provided for the soft electronic fish to show two different swimming speeds, and for fair comparison with other free-swimming robots, only the free-swimming version of the soft electronic fish was used (not the tethered version).

Robot	Mass (kg)	Speed (m/s)	External Power (W)	External Power per Mass (W/kg)
Biohybrid Robot (this work)	0.079 0.077 0.141	0.030 0.038 0.035	0.005 0.010 0.018	**0.06** **0.13** **0.12**
Artificial Ray (10)	0.010	0.003	0.010	**1.0**
Medusoid (9)	0.001	0.007	0.0016	**1.6**
Jennifish (33)	0.380	0.030	1.95	**5.1**
Soft Electronic Fish (7)	0.0903	0.011 0.031	0.5123 1.1100	**5.67** **12.29**
SoFi (34)	1.6	0.240	23.33	**14.6**
Robojelly (3)	0.242	0.031	17	**70**
REMUS 100 (35)	36	1.5	18000	**500**

Movie S1. A comparison of bell geometries for unstimulated swimming with an inactive swim controller embedded (left) and externally controlled swimming at 0.50 Hz (middle) and 0.88 Hz (right). Note that the full range of motion between bell contraction and relaxation does not occur at high frequencies (right).